



# The Role of Rho GTPases During Fibroblast Spreading, Migration, and Myofibroblast Differentiation in 3D Synthetic Fibrous Matrices

DANIEL L. MATERA,<sup>1</sup> ALEXANDER T. LEE,<sup>2</sup> HARRISON L. HIRAKI,<sup>3</sup> and BRENDON M. BAKER<sup>1,3</sup> 

<sup>1</sup>Department of Chemical Engineering, University of Michigan, Ann Arbor, MI 48109, USA; <sup>2</sup>Department of Biology, University of Michigan, Ann Arbor, MI 48109, USA; and <sup>3</sup>Department of Biomedical Engineering, University of Michigan, 2174 Lurie BME Building, 1101 Beal Avenue, Ann Arbor, MI 48109, USA

(Received 24 February 2021; accepted 9 August 2021; published online 2 September 2021)

Associate Editor Michael R. King oversaw the review of this article.

## Abstract

**Introduction**—Connective tissue repair and mechanosensing are tightly entwined *in vivo* and occur within a complex three-dimensional (3D), fibrous extracellular matrix (ECM). Typically driven by activated fibroblasts, wound repair involves well-defined steps of cell spreading, migration, proliferation, and fibrous ECM deposition. While the role of Rho GTPases in regulating these processes has been explored extensively in two-dimensional cell culture models, much less is known about their role in more physiologic, 3D environments.

**Methods**—We employed a 3D, fibrous and protease-sensitive hydrogel model of interstitial ECM to study the interplay between Rho GTPases and fibrous matrix cues in fibroblasts during wound healing.

**Results**—Modulating fiber density within protease-sensitive hydrogels, we confirmed previous findings that heightened fiber density promotes fibroblast spreading and proliferation. The presence of matrix fibers furthermore corresponded to increased cell migration speeds and macroscopic hydrogel contraction arising from fibroblast generated forces. During fibroblast spreading, Rac1 and RhoA GTPase activity proved crucial for fiber-mediated cell spreading and contact guidance along matrix fibers, while Cdc42 was dispensable. In contrast, interplay between RhoA, Rac1, and Cdc42 contributed to fiber-mediated myofibroblast differentiation and matrix contraction over longer time scales.

**Conclusion**—These observations may provide insights into tissue repair processes *in vivo* and motivate the incorporation of cell-adhesive fibers within synthetic hydrogels for material-guided wound repair strategies.

**Keywords**—Wound healing, Mechanosensing, Fibroblast, Myofibroblast, Cell migration, Synthetic hydrogels, Fibers, Microenvironment, Extracellular matrix, Electrospinning, Rho GTPase.

## INTRODUCTION

A 3D network of interpenetrating micron-scale fibers embedded within a finer meshwork of gel-like proteoglycans, the interstitial extracellular matrix (ECM) provides numerous structural and biochemical cues to drive cell and tissue function.<sup>19,70</sup> ECM homeostasis is maintained by fibroblasts, normally quiescent cells resident to the interstitial matrix of all organs in the body.<sup>5</sup> In response to external tissue damage, fibroblasts activate during the inflammatory phase of wound repair and migrate to the wound site, ultimately undergoing expansion and differentiation into myofibroblasts (MFs); these contractile cells mediate interstitial ECM deposition and reorganization during the latter phases of wound repair.<sup>5,12,33,75</sup> Insufficient recruitment and differentiation of MFs can hinder wound healing, and conversely, MF hyperactivity and resistance to apoptosis or dedifferentiation contribute to numerous pathologies such as organ fibrosis and cancer.<sup>33,77</sup> Consequently, understanding how interactions with the ECM influence fibroblast behavior is critical for both understanding pathophysiology and the creation of therapies that promote healthy wound repair.

While seminal work studying the wound healing response *in vivo* has been critical for characterizing the distinct phases, cellular players, and associated cytokines that mediate tissue repair,<sup>11,20,50</sup> limitations in intravital imaging and the lethality of genetic knockout of ECM proteins have hindered the study of fibroblast-ECM interactions at the cellular scale *in vivo*.<sup>10</sup> Consequently, *in vitro* studies of cells plated on 2D culture substrates have been critical for investigating fibroblast biology and in particular, matrix mechanosensing during the fibroblast wound healing

Address correspondence to Brendon M. Baker, Department of Biomedical Engineering, University of Michigan, 2174 Lurie BME Building, 1101 Beal Avenue, Ann Arbor, MI 48109, USA. Electronic mail: bambren@umich.edu

response. Multiple culture settings have noted the importance of cell adhesion and actomyosin force generation in the fibroblast-driven wound healing response.<sup>2,7,68</sup> These key fibroblast functions are controlled by the reorganization and force dynamics of the actomyosin cytoskeleton, dictated primarily by the activity of the Rho GTPases Rac1, Cdc42, and RhoA and their associated regulators.<sup>30,58,67</sup> Simple 2D models such as scratch wound assays have elucidated a requirement for RhoA and Rac1 in force generation and lamellipodia formation during cell migration, respectively, and the role of Cdc42 in proliferation and generating filopodia for cell-ECM sensing.<sup>38,40,46,58,67,76</sup> Given that these simple 2D models fail to recapitulate the 3D and fibrous nature of *in vivo* ECM, the use of reconstituted natural materials such as fibrin and type I collagen gels have also proved informative. Studies of fibroblasts embedded within these hydrogels further implicate Rho GTPases in wound healing processes, namely the requirement of RhoA for cell spreading and force generation required for macroscale gel contraction.<sup>29,80</sup> Importantly, while these natural hydrogels possess fibrous architecture, they lack a proteoglycan gel-like component, are prone to rapid degradation and resorption *in vivo* thus limiting their use for wound repair, and have biophysical properties that are difficult to modulate independently (e.g. increasing ECM protein concentration concomitantly increases fiber density, stiffness, and ligand density, but decreases pore size and degradability).<sup>22,37,57</sup> These material limitations have hindered the use of natural materials for mechanistic study of cell-ECM interaction, or for regenerative therapies which require stability across long time scales and tailored degradation rates.<sup>24,45</sup>

In contrast to naturally derived materials, synthetic hydrogels with tunable physical and biochemical properties have emerged as a powerful tool for dissecting the impact of individual matrix properties on cell function. For example, studies of fibroblasts seeded on non-degradable 2D hydrogels varying in stiffness suggest a requisite threshold of matrix stiffness and resulting RhoA/MRTF-A activity for MF differentiation.<sup>2,7</sup> Unfortunately, these synthetic polymeric networks typically lack micro-scale fibrous architecture and unlike native tissue ECM, possess a homogenous distribution of adhesive ligands and nanoporous topography.<sup>51,59</sup> Such distinctions raise concerns over whether results from these models translate to more complex *in vivo* tissue environments. Separately, electrospinning is an established method for fabricating fibrous scaffolds that have been widely investigated for wound repair applications, potentially indicating a positive influence of fibrous microstructure in wound healing.<sup>36,74</sup> Given that electrospun scaffolds are typi-

cally thin mats which lack a proteoglycan gel-like component and have subcellular pore sizes that limit cell infiltration,<sup>1</sup> we recently integrated electrospinning with cell-degradable hydrogel chemistries to generate a multi-component model of the extracellular matrix.<sup>44</sup> These fiber-hydrogel composites incorporate a tunable gel-like proteoglycan component and adhesive ligand-presenting microfibers, mimicking the two-phase structure of native ECM. Using this system, we recently showed that increased fiber density drives MF differentiation and fibrosis-associated signaling *in vitro*.<sup>42</sup> Given the parallels between wound healing and fibrosis, and furthermore the deposition of fibrous collagen occurring in both contexts,<sup>3,17</sup> we hypothesized that fiber-reinforced hydrogel composites would promote fibroblast functions associated with key phases of the wound healing process.

Here, we focused on the three primary phases of wound repair following hemostasis (ie. provisional matrix formation, cell proliferation and remodeling) with the goal of understanding how the interplay between Rho GTPase activity and a fibrous ECM cue facilitate the tissue repair functions of fibroblasts. In line with our previous data, the presence of cell-adhesive fibers induces earlier activation (spreading, stress fiber generation, migration and proliferation) of fibroblasts in 3D settings, and promotes MF differentiation ( $\alpha$ -smooth muscle actin ( $\alpha$ -SMA) expression and heightened contractility) at later timepoints. Via pharmacologic perturbation of RhoA, Rac1, and Cdc42, we then explored the intersection of Rho GTPase activity and cell-matrix fiber interactions that guide fibroblast spreading, migration, and differentiation toward MFs. Initial protrusion formation along matrix fibers was found to be Rac1 dependent in 3D, whereas maturation of these protrusions into stress fiber bearing structures required ROCK/RhoA. In contrast to prior results from 2D studies, we found that pharmacologic inhibition of Rac1 and Cdc42 had minimal effects on inhibiting the 3D migration of fibroblasts, whereas RhoA was essential. We also showed that inhibition of one GTPase alone was not sufficient to prevent MF differentiation at later timepoints. Our studies suggest a strong interplay between RhoA, Rac, and Cdc42 in 3D fibrous environments, and suggest that strategies to improve wound healing (or conversely prevent aberrant fibrosis) will likely need to simultaneously target multiple Rho GTPases in a cell function dependent manner.

## MATERIALS AND METHODS

### *Reagents*

All reagents were purchased from Sigma Aldrich and used as received, unless otherwise stated.

### *Synthesis and Characterization of Modified Dextran*

Dextran vinyl sulfone (DexVS) was synthesized using a previously established protocol for vinyl sulfonating polysaccharides adapted for use with high MW dextran (MW 86,000 Da, MP Biomedicals, Santa Ana, CA).<sup>13,44</sup> Briefly, pure divinyl sulfone (12.5 mL, Fisher Scientific, Hampton, NH) was added to a sodium hydroxide solution (0.1 M, 250 mL) containing dextran (5 g). This reaction was carried out at 1500 RPM for 3.5 min, after which the reaction was terminated by adjusting the pH to 5.0 via the addition of hydrochloric acid. A lower functionalization of DexVS was utilized for hydrogels, where the volume of divinyl sulfone reagent was reduced to 3.875 mL. All reaction products were dialyzed for 5 days against Milli-Q ultrapure water, with two water exchanges daily, and then lyophilized for 3 days to obtain the pure product. Functionalization of DexVS was characterized by <sup>1</sup>H-NMR spectroscopy in D<sub>2</sub>O and was calculated as the ratio of the proton integral (6.91 ppm) and the anomeric proton of the glucopyranosyl ring (5.166 and 4.923 ppm); here a vinyl sulfone/dextran repeat unit ratio of 0.376 and 0.156 was determined for electrospinning and hydrogel DexVS polymers, respectively.

### *Fiber Segment Fabrication*

DexVS was dissolved at 0.6 g mL<sup>-1</sup> in a 1:1 mixture of Milli-Q ultrapure water and dimethylformamide with 0.015% Irgacure 2959 photoinitiator. Methacrylated rhodamine (0.5 mM; Polysciences, Inc., Warrington, PA) was incorporated into the electrospinning solution to fluorescently visualize fibers. This polymer solution was utilized for electrospinning within an environment-controlled glovebox held at 21 °C and 30% relative humidity. Electrospinning was performed at a flow rate of 0.3 mL h<sup>-1</sup>, gap distance of 5 cm, and voltage of -10.0 kV onto a grounded collecting surface attached to a linear actuator. Fiber layers were collected on glass slabs and primary crosslinked under ultraviolet light (100 mW cm<sup>-2</sup>) and then secondary crosslinked (100 mW cm<sup>-2</sup>) in a 1 mg mL<sup>-1</sup> Irgacure 2959 solution. After polymerization, fiber segments were resuspended in a known volume of PBS (typically 3 mL). The total volume of fibers was then calculated via a conservation of volume equation: total resulting solution volume = volume of fibers + volume of PBS

(3 mL). After calculating total fiber volume, solutions were re-centrifuged, supernatant was removed, and fiber pellets were resuspended to create a 1.1 vol% fiber solution, which were then aliquoted and stored at 4 °C. To support cell adhesion, 2.0 mM RGD (CGRGDS, Genscript, Piscataway, NJ), was coupled to vinyl sulfone groups along the DexVS backbone via Michael-type addition chemistry for 30 min, followed by quenching of excess VS groups in a 300 mM cysteine solution for 30 min. To remove free thiols after quenching, fiber solutions were vigorously rinsed via flushing with excess PBS three times before use in cell studies.

### *Hydrogel Formation*

DexVS gels were formed via a thiol-ene click reaction at 3.3% w/v (pH 7.4, 37 °C, 45 min) with VPMS crosslinker (12.5mM) (GCRDVPMSMRGGDRCG, Genscript) in the presence of heparin-binding peptide (HBP, GCGAFAKLAARLYRKA, 0.65 mM, Genscript), and fiber segments (0.0–2.5% v/v). Cysteine was added to precursor solutions to maintain a final vinyl sulfone concentration of 60 mM after gelation. All hydrogel and peptide precursor solutions were made in PBS containing 50 mM HEPES. To create fibrous hydrogels, a defined stock solution (10% v/v) of suspended fibers in PBS/HEPES was mixed into hydrogel precursor solutions prior to gelation. For gel contraction experiments, DexVS was polymerized within a gelatin-coated 5 mm diameter PDMS gasket to ensure consistent hydrogel area beginning on day 0.

### *Cell Culture and Biological Reagents*

Normal human lung fibroblasts (University of Michigan Central Biorepository) were cultured in DMEM containing 1% penicillin/streptomycin, L-glutamine and 10% fetal bovine serum (Atlanta Biologics, Flowery Branch, GA). Cells were passaged upon achieving 90% confluency at a 1:4 ratio and used for studies until passage 7. For all hydrogel studies, cells were detached with 0.05% trypsin-EDTA (Life Technologies), counted and encapsulated into 12.5 μL hydrogels at a density of 1,000,000 cells mL<sup>-1</sup> of hydrogel, and subsequently cultured at 37 °C and 5% CO<sub>2</sub> in serum containing medium. For 2D studies of cell morphology F-actin organization (Supplementary Fig. 1), the total number of cells seeded onto each 12 mm glass coverslip was equivalent to 12.5 μL hydrogels described above. Media was refreshed the day after encapsulation and every 2 days after. For migration studies, fibroblasts were trypsinized (0.05%), counted, formed into 300 cell aggregates overnight in an AggreWell<sup>TM</sup> (STEMCELL Technologies, Vancouver,

BC, Canada) substrate treated with 0.5% pluronic F-127 to prevent cell adhesion, and encapsulated into DexVS hydrogels after 24 h. In differentiation experiments, recombinant human TGF- $\beta$ 1 (Peprotech, Rocky Hill, NJ) was supplemented to media at 5 ng mL<sup>-1</sup>. For pharmacological studies, Y-27632 (30  $\mu$ M, Fisher Scientific, Hampton, NH), NSC-27366 (50  $\mu$ M, Fisher Scientific, Hampton, NH), ML141 (20  $\mu$ M), and LPA (15  $\mu$ M), were supplemented to media and refreshed every 2 days.

#### *Fluorescent Staining, Microscopy, and Analysis*

Cultures were fixed with 4% paraformaldehyde for 30 min at room temperature. To stain the actin cytoskeleton and nuclei, samples were permeabilized in PBS solution containing Triton X-100 (0.5% v/v), sucrose (10% w/v), and magnesium chloride (0.6% w/v), blocked in 1% BSA, and stained simultaneously with phalloidin and DAPI. For immunostaining, samples were permeabilized, blocked for 8 h in 1% w/v bovine serum albumin, and incubated with mouse monoclonal anti- $\alpha$ -SMA (1:2000, Sigma #A2547) or rabbit monoclonal anti-Ki67 (1:500, Sigma-Aldrich #PIMA514520) followed by secondary antibody for 6 h each at room temperature with 3x PBS washes in between. All samples were imaged on a Zeiss LSM 800 laser scanning confocal microscope. High-resolution images of F-actin were acquired with a 40x water-immersion objective. Unless otherwise specified, images are presented as maximum intensity Z-projections of 25 (Fig. 2), 50 (Fig. 4), 100 (Figs. 1, 5) or 300  $\mu$ m (Fig. 3) Z-stacks, respectively. Single cell morphometric analyses (cell aspect ratio) were performed using custom Matlab scripts with sample sizes > 25 cells/group, while total F-actin spread area,  $\alpha$ -SMA, and Ki67 were quantified on an image basis with a minimum of 10 distinct fields of view. 3D migration characteristics were determined via custom Matlab scripts utilizing  $n > 10$  fibroblast aggregates/group, with invasion defined as nucleated F-actin+ structures with aspect ratio > 2. Migration heatmaps are presented as an overlay of all biological replicates. Myofibroblasts were denoted as nucleated, F-actin<sup>+</sup>,  $\alpha$ -SMA<sup>+</sup> cells. For cell density (# of nuclei) measurements, DAPI-stained cell nuclei were thresholded and counted in six separate 600  $\times$  600  $\times$  200  $\mu$ m image volumes, allowing us to calculate a total number of cells per mm<sup>3</sup> of gel. The percent of  $\alpha$ -SMA<sup>+</sup> cells was determined via a custom Matlab script; briefly, cell outlines were created via thresholding  $\alpha$ -SMA images and the total number of nuclei were quantified under each  $\alpha$ -SMA mask on a per image basis. A similar analysis method in Matlab was used on F-actin for area:perimeter ratio measurement, as published previ-

ously, where higher area:perimeter ratios indicate the formation of a more interconnected, multicellular network.<sup>14</sup>

#### *Mechanical Testing*

To determine the elastic modulus of DexVS hydrogels, indentation tests were performed with a Nanosurf FlexBio atomic force microscope (AFM; Nanosurf, Liestal, Switzerland). Samples were indented with a 5  $\mu$ m diameter colloidal probe tip (spring constant = 0.03 N/m) to a depth of 10  $\mu$ m at a rate of 0.333  $\mu$ m/s. Resulting force-displacement curves were fit to a spherical Hertz model utilizing AtomicJ, assuming a Poisson's ratio of 0.5.

#### *Statistical Analysis*

Statistical significance was determined by one-way and two-way analysis of variance (ANOVA) or Student's *t*-test where appropriate, with significance determined by  $p < 0.05$ . All data are presented as a mean  $\pm$  standard deviation.

## RESULTS

### *Fabrication of Fiber-Reinforced Hydrogel Composites as a Model of Late Provisional Matrix*

Given the 3D nature of many native tissues, the nearly ubiquitous presence of ECM fibers *in vivo*, and the importance of fibronectin and collagen secretion during the production of provisional matrix,<sup>3</sup> here we utilized a previously established strategy to generate a 3D fibrous hydrogel model of the wound environment. To generate cell-adhesive, micron-scale diameter ECM-like fibers, we functionalized dextran, a protein adsorption-resistant hydrophilic polysaccharide amenable to electrospinning, with pendant vinyl sulfone groups that support photo-crosslinking and peptide functionalization through UV-initiated radical polymerization and Michael-type addition, respectively. We then electrospun dextran vinyl sulfone (DexVS) on a cylindrical collection mandrel (Fig. 1a) to optimize collection efficiency of deposited  $\sim$ 1  $\mu$ m diameter DexVS fibers. These fibers were then UV photo-crosslinked, collected in suspension, and functionalized with the adhesive ligand RGD (CGRGDS), an integrin-binding ligand that supports cell spreading, a process critical to wound healing.<sup>4,65,72</sup> After RGD functionalization, DexVS fibers were encapsulated within a DexVS hydrogel crosslinked with thiolated matrix-metalloproteinase (MMP) cleavable peptides (GCVPMS↓MRGGCG), yielding a two-phase com-

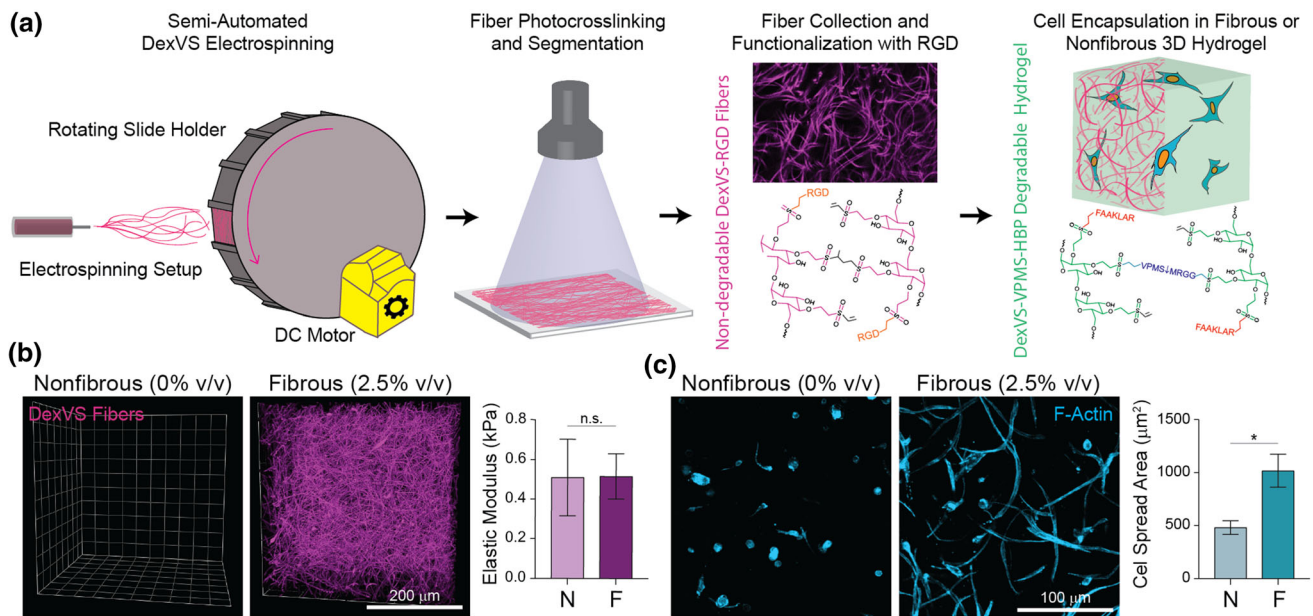


**FIGURE 1.** Synthetic fibrous hydrogel composites to model the late provisional matrix of wound healing. (a) Fabrication schematic for generating fiber-reinforced DexVS hydrogels. (b) Representative confocal Z-stack renderings of a nonfibrous (N, 0.0% volume) and high fiber density hydrogel (F, 2.5% volume), with rhodamine-tagged fibers in magenta (scale bar: 200  $\mu\text{m}$ ). Young's modulus determined by AFM nanoindentation of control and fibrous DexVS hydrogels ( $n = 4$  samples/group,  $n = 5$  indentations/sample). (c) Representative images of fibroblast F-actin (cyan) within control and fibrous DexVS hydrogels 24 h after encapsulation, with quantification of projected cell spread area ( $n = 4$  samples/group,  $n = 10$  fields of view/group,  $n > 25$  cells/field of view; scale bars: 100  $\mu\text{m}$ ). All data presented are means  $\pm$  standard deviations; asterisk denotes significance with  $p < 0.05$  determined by a Student's *t*-test.

posite of cell-adhesive, non-degradable matrix fibers ensconced within protease-degradable hydrogel. Given the importance of matrix deposition during wound repair, we also functionalized the hydrogel component with a heparin-binding peptide (HBP, CGFAKLAARLYRKAG) to sequester fibroblast-secreted proteins that interact with heparan sulfate proteoglycans.<sup>49</sup>

This material platform allows for orthogonal modulation of fiber density (0–2.5% volume fibers) without altering the elastic modulus or degradation kinetics of the surrounding bulk hydrogel (Fig. 1b). Due to the non-degradable nature of DexVS fibers, this system also maintains constant RGD density despite surrounding hydrogel degradation, making this platform advantageous for studying fibroblast-ECM interactions during the wound healing process. Primary human fibroblasts encapsulated in DexVS hydrogels containing a fiber density reflecting late provisional matrix stimulated a cell spreading response after 24 h of culture, whereas fibroblasts within control, nonfibrous hydrogels remained largely unspread over the same period. These results are in line with findings from our prior work showing that fibrous microstructure expedites cell spreading and adhesion-mediated signaling required for fibroblast activation.<sup>42</sup> Given the ubiquity of fibrous interstitial ECM and the

well-documented role of matrix fiber remodeling in the later phases of wound repair,<sup>3,79</sup> we compared cell behavior in nonfibrous DexVS hydrogels vs. fibrous composites, with the goal of understanding how Rho GTPase activity in fibroblasts mediates cell interactions with matrix fibers and resultant fibroblast function.

#### *Dissecting the Role of ROCK, Rac1, and Cdc42 in Fibroblast Activation During the Early Stages of Wound Repair*

In response to inflammatory cues arising from tissue damage, one of the earliest stages of fibroblast activation *in vivo* is altered cell morphology and the generation of actin stress fibers.<sup>11,26,71,47</sup> Consequently, we first investigated how the presence of matrix fibers modulates normal human lung fibroblast morphology through high-resolution confocal microscopy. In line with our prior results, fibers induced rapid spreading over 24 h in DexVS hydrogels, primarily through contact guidance of nascent cellular protrusions (thin finger-like structures that ultimately develop into F-actin rich extensions) along adjacent fibers (Fig. 2a, white arrows). Fiber-mediated spreading led to increased cellular spread areas as quantified by F-actin staining (Fig. 2b), and a spindle-like cytoskeletal

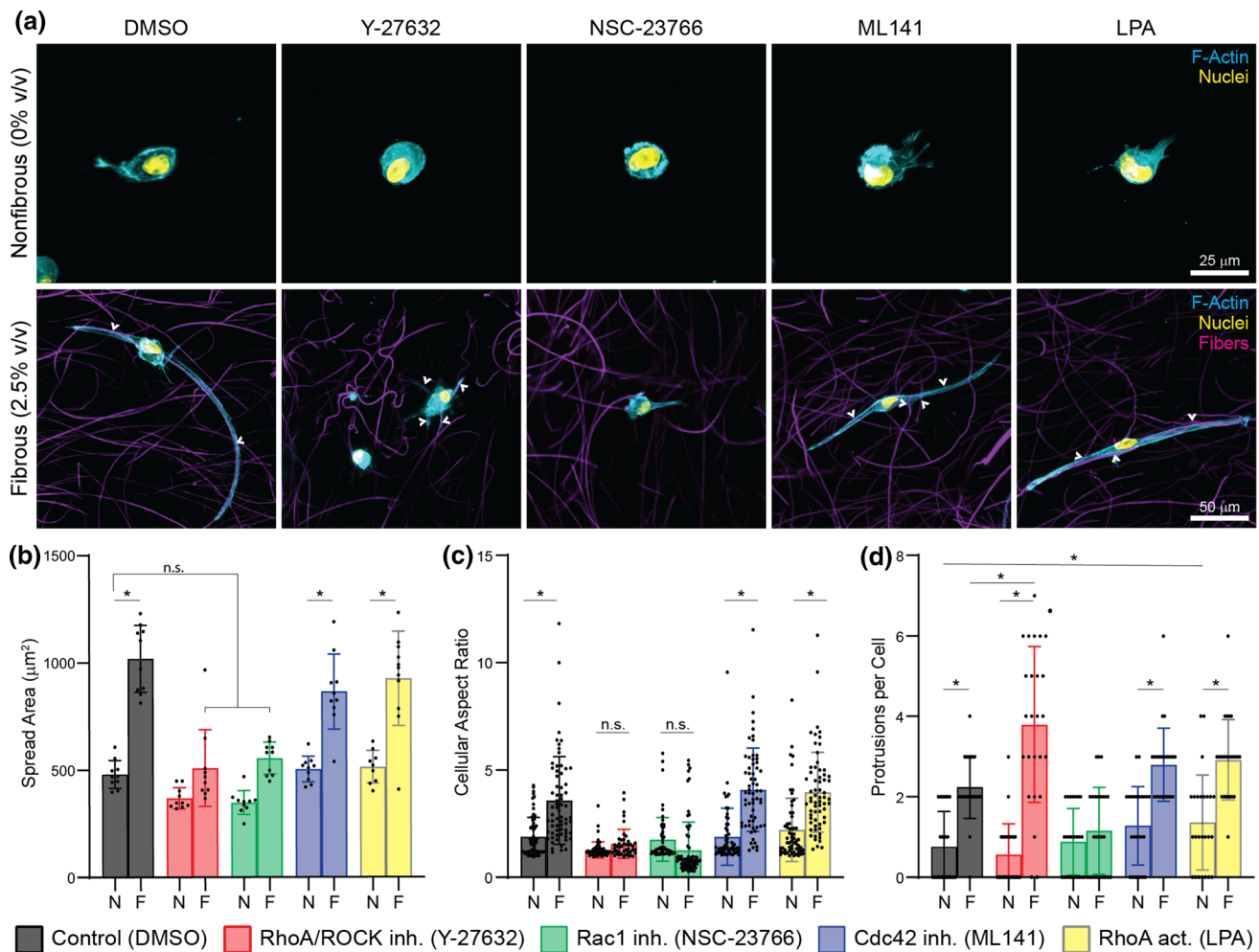


**FIGURE 2.** Fiber-mediated cell spreading as a function of pharmacologic modulation of Rho GTPases. (a) High-resolution images of fibroblasts in nonfibrous (N, 0.0% v/v) and fibrous (F, 2.5% v/v) DexVS hydrogels after 24 h of culture in the presence of denoted pharmacologic modulators or DMSO (F-actin (cyan), nuclei (yellow), DexVS fibers (magenta); scale bars: 50  $\mu\text{m}$ ). White arrows denote arrows of contact guidance along DexVS fibers. Corresponding image quantification of projected (b) F-actin cell spread area, (c) cell aspect ratio, and (d) total number of protrusions per cell ( $n = 4$  samples/group; for aspect ratio and protrusion quantification,  $n > 25$  cells/group; for spread area  $n > 10$  fields of view/group and  $n > 25$  cells/field of view). Protrusions were defined as F-actin rich puncta greater than 5  $\mu\text{m}$  in length. All data presented are means  $\pm$  standard deviations; asterisk denotes significance with  $p < 0.05$  determined by a two-way analysis of variance.

morphology with high aspect ratios (Fig. 2d) frequently driven by two dominant actin-rich protrusions (Fig. 2a). In contrast, fibroblasts in control gels possessed high levels of cortical actin and small, randomly oriented protrusions which were fewer in number, resulting in lower spread areas and cellular aspect ratios (Figs. 2a–2d).

To explore which Rho family GTPases are required for cell interactions with matrix fibers and ensuing changes in cell morphology, we treated fibroblasts embedded in nonfibrous and fibrous DexVS hydrogels with a panel of pharmacologic modulators for 24 h: Y-27632 to reduce the activity of Rho-associated protein kinase (ROCK), the primary downstream effector of RhoA; NSC-23766 to reduce Rac1 activity; ML141 to reduce Cdc42 activity; and lysophosphatidic acid

(LPA), a RhoA agonist. Pharmacologic concentrations were validated via screening on 2D tissue culture plastic over ranges known to impact cellular morphology (Supplemental Fig. 1A). Reduction of ROCK activity reduced fiber-induced increases in total cellular spread area and aspect ratio (Figs. 2b, 2c) although interestingly, we noted an increase in the number of protrusions (Figs. 2a arrows, 2d), suggesting that ROCK activity is not required for the initiation of protrusions and their extension along matrix fibers. Diminished spreading despite greater number of protrusions, suggests that ROCK activity may be required for maturing nascent protrusions through actin polymerization and eventual actin stress fiber formation. In contrast, reduction of Rac1 activity via NSC-23766 treatment inhibited fiber-mediated cell spreading

through a distinct mechanism. NSC-23766 treatment abrogated increases in protrusion formation due to the presence of fibers (Figs. 2a, 2d), leading to decreased cell spreading, lower aspect ratios, and cell morphologies akin to cells within nonfibrous hydrogels. ML141 and LPA treatment to reduce Cdc42 activity and activate RhoA, respectively, did not have detectable effects on cell spread area, aspect ratio, or protrusion formation. These results suggest that contact guidance and protrusion formation are not Cdc42 dependent in 3D for human fibroblasts, in contrast to in 2D culture where we detected fewer protrusions in ML141 treated conditions (Supplemental Fig. 1A). Furthermore, the insignificant effects of LPA treatment in fibrous conditions suggests that while RhoA/ROCK activity is required for fiber-induced maturation of protrusions and subsequent spreading in 3D, levels of RhoA activity are not limiting in these settings.

While cell adhesion, spreading, and underlying cytoskeletal dynamics are often thought to be initial steps for fibroblast activation in response to inflammation and tissue damage, subsequent cell migration and infiltration into the wound bed is critical for wound healing and may also contribute to tissue fibrosis in pathologic contexts.<sup>69</sup> To explore how matrix fibers affect fibroblast migration and to determine which Rho GTPases are critical for this process in 3D, we established a migration assay whereby spheroidal fibroblast aggregates ( $\varnothing = 300 \mu\text{m}$ ) were encapsulated in control and fibrous hydrogels, stimulated with serum for 24 h, and exposed to pharmacologic modulators for the next 4 days prior to analysis. In control gels without pharmacologic treatment, we observed nearly a three-fold increase in the total number of migratory invasion events (defined as single or multicellular fibroblast strands infiltrating the hydrogel) in fibrous conditions compared to nonfibrous hydrogels (Figs. 3a, 3b), supporting numerous observations that fibrous contact guidance cues support cell polarization and subsequent migration in 3D hydrogel environments.<sup>55,66,78</sup> Corresponding to this, we also observed an increase in the total invasion area (determined from total F-actin area outside of the initial cell aggregate, Fig. 3c) and average migration distance (Fig. 3d) in fibrous conditions, suggesting that fibrous matrix cues also supported more extensive migration in actively motile cells.

Treatment with Y-27632 led to increases in invasion events across all hydrogel conditions (Figs. 3a, 3b), supporting our earlier observation that protrusion formation does not appear to be ROCK dependent (Fig. 2). However, it should be noted that while an increased number of actin-rich protrusions extended into the surrounding hydrogel, cells were unable to

migrate away from the aggregate periphery (Figs. 3c, 3d), suggesting that ROCK-dependent contractile forces are required for migration in 3D following protrusion formation. Supporting this hypothesis, LPA treatment to activate RhoA/ROCK signaling increased total migration distances in nonfibrous hydrogels and migration areas in fibrous composites, but did not influence the total number of invasion events. While inhibition of Rac1 via NSC-23766 treatment appeared to have limited effects on cell migration in nonfibrous gels, a reduced number of migratory events, invasion area, and invasion distance were observed in fibrous gels (Figs. 3a–3d). Given that Rac1 inhibition also blocked fiber-guided protrusions during cell spreading (Fig. 2), these results further suggest that Rac1 is a key player during cell-fiber contact guidance and initial protrusion formation. ML141 treatment conversely led to increased migration areas and distances in all conditions, and also increased the total number of migratory events in nonfibrous conditions. Interestingly, Cdc42 has well-known roles in filipodia generation and sensing processes that impact 2D migration. Taken together, these results suggest both ROCK and Rac1 are required for migration in 3D, where Rac1 aids in initial protrusion formation after which ROCK activity is required for the generation of actomyosin-mediated forces and subsequent translocation of the cell body.

#### *Dissecting the Role of ROCK, Rac1, and Cdc42 in Fibroblast Behavior During the Proliferative Phase of Wound Repair*

While fibroblasts migrate into provisional matrix soon after injury, the ensuing proliferative phase of wound healing requires proliferation of recruited fibroblasts to create a hypercellular repair tissue reinforced by cell-cell junctions.<sup>64,69</sup> Through cadherins, these multicellular networks function to drive the coordination of cell-generated tensile forces across long distances in the wound bed to mediate tissue contraction.<sup>18,28,53</sup> Previous data from our lab suggests that fibroblast assembly into multicellular networks precedes myofibroblast (MF) differentiation and resulting matrix contraction, all of which were enhanced in the presence of matrix fibers.<sup>42</sup> Given that multicellular network formation likely occurs through iterative rounds of protrusive activity, cell spreading, and proliferation, we hypothesized that Rho GTPases underlie the transition from solely cell-ECM adhesion to a mixture of cell-ECM and cell-cell adhesion. Consequently, we sparsely encapsulated single fibroblasts within nonfibrous control and fibrous DexVS hydrogels to explore how RhoA/ROCK, Rac1, and Cdc42 activity affect fibroblast proliferation and mul-

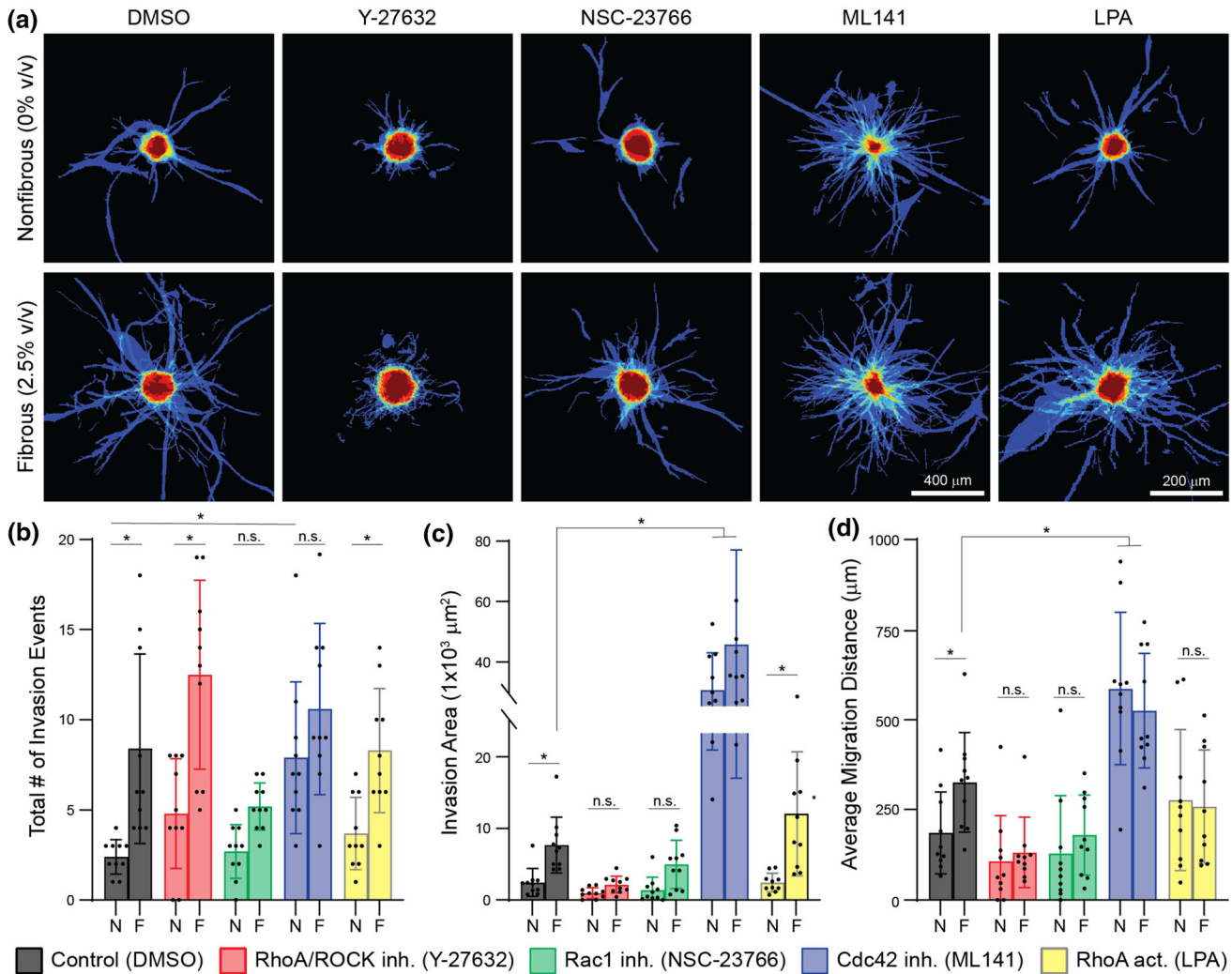


**FIGURE 3.** Fiber-mediated cell migration as a function of pharmacologic modulation of Rho GTPases. (a) Heat map overlays created by an aggregate sum of binarized F-actin images of migrating fibroblast aggregates, after exposure to denoted pharmacologic modulators or DMSO vehicle control for 4 days ( $n = 10$  spheroids/overlay). Red regions indicate regions of greater similarity between replicates, typically denoting the body of the fibroblast aggregate where migration originated from (scale bars: 200  $\mu\text{m}$  for DMSO, Y-27632, NSC-23766, and LPA treated conditions or 400  $\mu\text{m}$  in ML141 treated conditions). Corresponding image quantification of the (b) total number of migration events, (c) invasion area, and (d) migration distance ( $n > 10$  aggregates analyzed/group). Migration events were defined as single or collective groups of cells migrating out of the encapsulated fibroblast aggregate (seen in red in heat map overlays). Migration distance was calculated as the distance from the centroid of each migrating cell or multicellular cluster to the center of the aggregate body. All data presented are means  $\pm$  standard deviations; asterisk denotes significance with  $p < 0.05$  determined by a two-way analysis of variance.

ticellular network formation over 5 days of culture. Supporting our prior data,<sup>42</sup> the incorporation of fibers promoted proliferation (Figs. 4a, 4d) and network formation, as quantified by a nearly three-fold increase in network area and area:perimeter (A/P) ratio (Figs. 4a–4c), a metric commonly used for vasculogenesis assays where a higher ratio denotes a more interconnected multicellular structure.<sup>6,14</sup>

ROCK and Rac1 inhibition markedly reduced fiber-mediated proliferation and network formation (Fig. 4), although potentially via different mechanisms. Fibroblasts treated with Y-27632 appeared to form

more protrusions as observed in early cell spreading studies (Fig. 2), leading to networks with an excess of branch points but less robust junctional assembly between neighboring cells overall (Supplementary Fig. 1C). In contrast, fibroblasts treated with NSC-23766 appeared to extend unidirectionally along fibers, but the lack of proliferation led to infrequent cell-cell contact and overall limited network formation. Furthermore, in instances where cell-cell contact occurred in NSC-23766 treated fibrous conditions, junctional reinforcement appeared limited as evidenced by thinner F-actin connections between cells (Supplementary

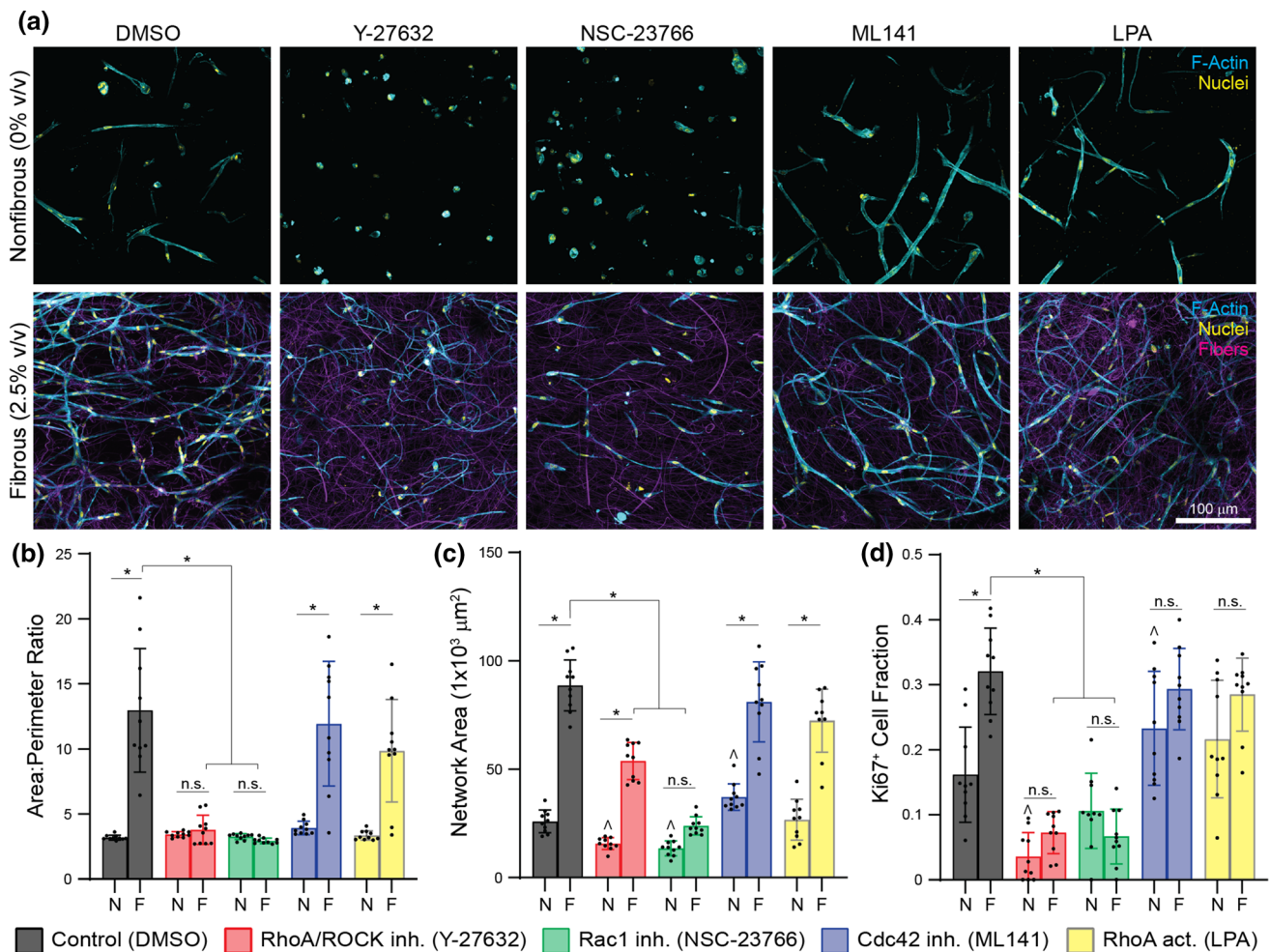


**FIGURE 4.** Fiber-mediated multicellular network assembly as a function of pharmacologic modulation of Rho GTPases. (a) High-magnification images of fibroblast morphology and network formation in nonfibrous and fibrous DexVS hydrogels, after 5 days of culture in the presence of denoted pharmacologic modulators or DMSO (F-actin (cyan), nuclei (yellow), DexVS fibers (magenta); scale bars: 100 μm). Corresponding image quantification of (b) F-actin cellular A/P ratio, (c) F-actin network area, and (d) the fraction of Ki67+ cells within each network ( $n = 4$  samples/group; area  $n > 10$  fields of view/group and  $n > 25$  cells/field of view). Ki67+ cells were defined as cells with co-localization of Ki67 and DAPI. All data presented are means  $\pm$  standard deviations; asterisk denotes significance with  $p < 0.05$  determined by a two-way analysis of variance; ^denotes significance relative to DMSO containing conditions as determined via a post hoc Dunnett's multiple comparison test.

Fig. 1C). However, given the reduced rates of cell proliferation across ROCK and Rac1 inhibited conditions and the importance of proliferation for multicellular network formation, it is difficult to speculate whether diminished cell density and/or fiber-dependent spreading and cell migration are behind the reduction in multicellular assembly.

In nonfibrous conditions, treatment with Y-27632 and NSC-23766 both abrogated cell spreading and reduced total network area (Fig. 4), suggesting that ROCK and Rac1 activity are also critical for cell spreading in nonfibrous hydrogel environments where guidance cues are lacking. In contrast, treatment with ML141 increased proliferation (Fig. 4d) and network area in nonfibrous control hydrogels, suggesting that Cdc42 activity may actually have an inhibitory role on

cell spreading in nonfibrous DexVS hydrogels. Interestingly, Cdc42 activity was dispensable for network formation in fibrous hydrogels, paralleling observations of initial cell spreading at day 1. In sum, these results support prior data (Fig. 2) suggesting that an interplay between Rac1 (required for cell-fiber contact guidance and cell-cell junction formation) and ROCK (required for the development of nascent protrusions into larger spindle structures, contractility, and effective migration) are both critical for fibroblast activation processes in 3D.

Activated fibroblasts possess stress fibers and migratory capacity, and more frequently undergo cell division during the inflammatory and proliferative stages of wound healing. However, their differentiation towards highly contractile  $\alpha$ -SMA<sup>+</sup> myofibroblasts

coincides with the initiation of the remodeling phase, marked by ECM synthesis and tissue contraction.<sup>27</sup> Thus, here we explored whether ROCK, Rac1, or Cdc42 activity were critical for MF differentiation in 3D fibrous environments. Fibroblasts were encapsulated in nonfibrous control and fibrous hydrogels (day 0), allowed 24 h for spreading, and then culture media was supplemented with the profibrotic cytokine TGF- $\beta$ 1 (days 1-9), given its pleiotropic roles during wound healing and MF differentiation *in vivo*.<sup>61</sup> Indeed, TGF- $\beta$ 1 supplementation was necessary for MF differentiation in DexVS hydrogels regardless of the presence of fibers (Figs. 5a, 5b), although matrix fibers synergized with TGF- $\beta$ 1 to increase fibroblast proliferation

(Fig. 5c) and the appearance of  $\alpha$ -SMA<sup>+</sup> MFs (Fig. 5b), as we have previously reported.<sup>42</sup>

To account for the significant variation in proliferation rates across pharmacologic treatments observed in previous experiments (Fig. 4), we allowed fibroblasts to spread, proliferate, and form multicellular networks prior to the introduction of cytoskeletal modulators on days 5–9. ROCK, Rac1, or Cdc42 inhibition all reduced MF differentiation in fibrous composites, although not to levels of nonfibrous controls (Figs. 5a, 5b). As evidenced by low A/P ratios in nonfibrous conditions (Fig. 5c), limited multicellular network formation may be another reason why MF differentiation was limited in the absence of fibers. Indeed, A/P ratios were also reduced in treatment conditions with

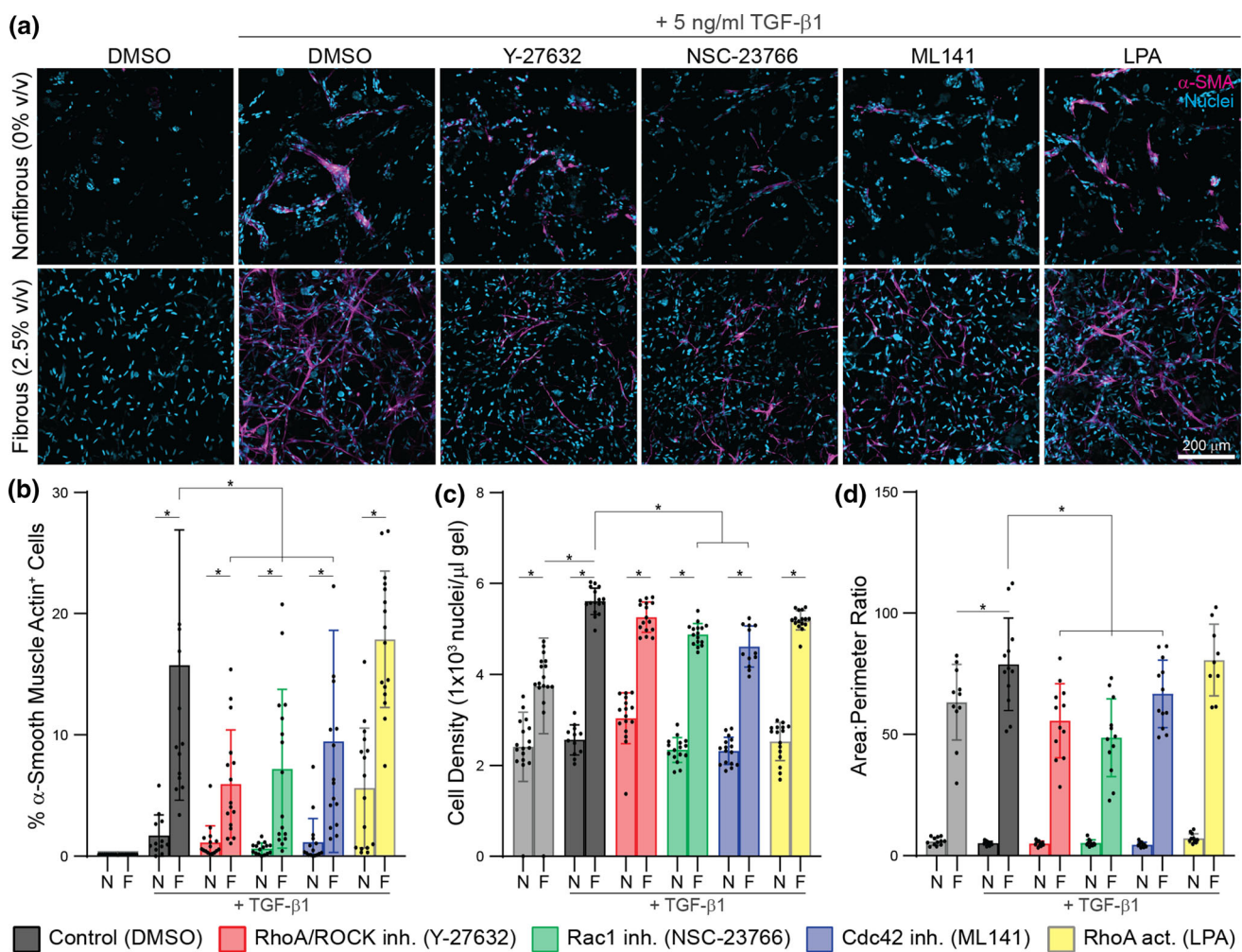


**FIGURE 5.** Fiber-mediated myofibroblast differentiation as a function of pharmacologic modulation of Rho GTPases. (a) Confocal images of the myofibroblast marker  $\alpha$ -SMA within nonfibrous and fibrous DexVS hydrogels after 9 days of culture in the presence of stimulatory cytokine TGF- $\beta$ 1 or control media. Starting on day 5 after network formation, cultures were exposed to denoted pharmacologic modulators or DMSO until fixation ( $\alpha$ -SMA (magenta), nuclei (cyan); scale bars: 400  $\mu$ m). Corresponding image quantification of (b)  $\alpha$ -SMA<sup>+</sup> cells, (c) total nuclei, and (d) F-actin area:perimeter ratio ( $n = 4$  samples/group; area  $n > 10$  fields of view/group and  $n > 800$  cells/field of view).  $\alpha$ -SMA<sup>+</sup> cells were defined as cells with co-localization of F-actin and  $\alpha$ -SMA. All data presented are means  $\pm$  standard deviations; asterisk denotes significance with  $p < 0.05$  determined by a two-way analysis of variance. Significance relative to TGF- $\beta$ 1 containing conditions was determined via a post hoc Dunnett's multiple comparison test.

lower  $\alpha$ -SMA<sup>+</sup> fibroblasts in fibrous gels (Fig. 5c), further associating multicellular network formation with MF differentiation. In summary, these results suggest that while ROCK and Rac1 inhibition are effective in reducing fiber-mediated contact guidance (Fig. 2), migration (Fig. 3), and proliferation/network formation (Fig. 4) in fibroblasts, their targeting alone is not sufficient to completely inhibit MF differentiation once fibroblast networks have formed. Furthermore, these results are consistent with various *in vivo* models showing that Rac1, ROCK, and Cdc42 activity are all critical for wound closure and organ fibrosis,<sup>16,39,40,54,63</sup> yet contrast work showing enhanced MF differentiation with Rac1 ablation *in vitro*.<sup>21,32</sup> However, given that Rac1 inhibition has also been shown to inhibit MF differentiation in other contexts,<sup>8,62</sup> it is likely that Rac1 has differing effects as a function of cell type and culture setting.

While proliferation followed by  $\alpha$ -SMA expression are accepted markers of differentiated MFs, these cells functionally contribute to wound repair in part through macroscale tissue contraction and resultant closure of wound margins. To explore how modulation of ROCK, Rac1, and Cdc42 activity affect the contractile function of MFs over longer time scales, we repeated the prior experiment but detached hydrogels from underlying tissue culture plastic, creating free-floating hydrogels amenable to bulk contraction. Given the limited MF differentiation and proliferation observed in nonfibrous DexVS hydrogels, only fibrous conditions were explored in this study. As expected, hydrogel contraction was enhanced with TGF- $\beta$ 1 supplementation as evidenced by lower final hydrogel areas on day 14 (Fig. 6). Unexpectedly, however, nearly all treatment conditions (Y-27632, NSC-23766, ML141) reduced hydrogel contraction to levels seen in control conditions lacking exogenously added TGF- $\beta$ 1, despite the fact that MFs were detected in Y-27632, NSC-23766, and ML141 treated samples by day 9 (Fig. 5). Furthermore, given that hydrogel contraction still occurred in conditions lacking TGF- $\beta$ 1, where differentiated MFs were undetectable, these data suggest that the capacity of fibroblasts to contract tissues is not fully dependent  $\alpha$ -SMA expression, and that inhibition of ROCK, Rac1, and Cdc42 is sufficient to diminish the contractility of undifferentiated fibroblasts. This is in contrast to the literature suggesting that RhoA/ROCK activity is the primary driver of fibroblast contraction and force generation in 2D,<sup>30,48</sup> but perhaps is not surprising given the well-known role of Rac1 and Cdc42 in regulating actin polymerization and cell-cell adhesion in other contexts.<sup>67</sup>

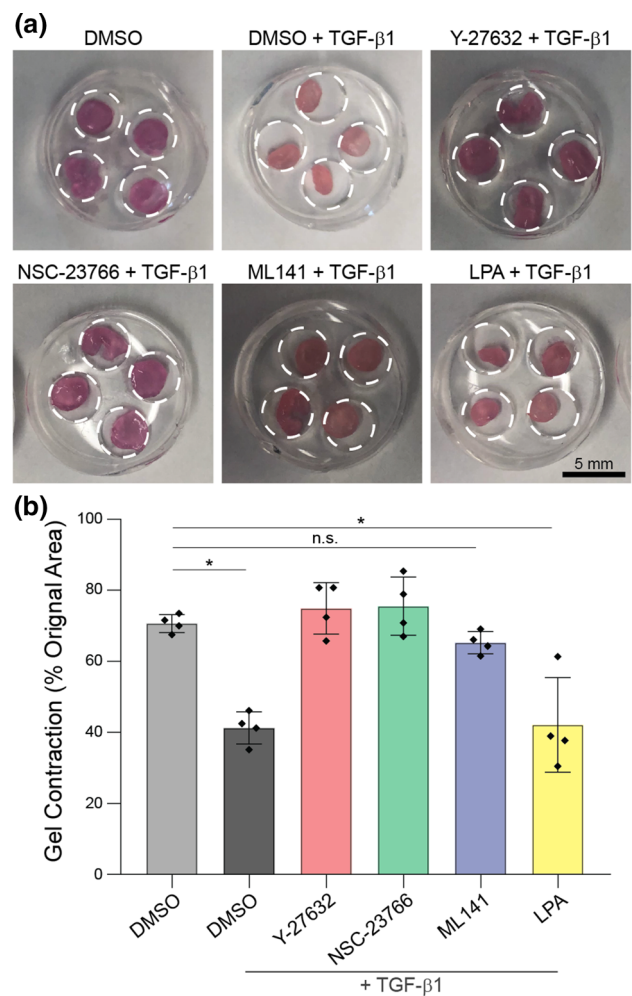


**FIGURE 6. Fiber-mediated hydrogel contraction as a function of pharmacologic modulation of Rho GTPases. (a) Macroscopic images of a DexVS contraction assay after 14 days of culture in the presence of stimulatory cytokine TGF- $\beta$ 1 or media control. Starting on day 5, cultures were exposed to denoted pharmacologic modulators or DMSO vehicle control until fixation. Dashed line surrounding each hydrogel gasket has a 15 mm diameter. (b) Corresponding image quantification of DeXS hydrogel contraction on day 14 ( $n = 4$  25ul hydrogels per group). All data presented are means  $\pm$  standard deviations; asterisk denotes significance with  $p < 0.05$  determined by a one-way analysis of variance.**

## DISCUSSION

Despite the critical role of wound healing processes during tissue homeostasis and fibrotic diseases, few studies have investigated the interplay between the fibrous structure present in provisional matrix and key cytoskeletal regulators in 3D microenvironments.<sup>3,35</sup> Wound healing models *in vitro* are most frequently protease-independent 2D scratch wound assays lacking fibrous microstructure, or alternatively reconstituted collagen gels that lack a proteoglycan component and have limited tunability.<sup>38,51</sup> To address this, here we leveraged electrospinning and hydrogel chemistries to

generate a biomimetic model of provisional matrix; this synthetic approach allowed us to define the density of matrix fibers without affecting initial 3D hydrogel stiffness or degradability, factors that are determined by the gel-like proteoglycan component. Pairing this approach with well-characterized pharmacologies allowed us to dissect the interplay between Rho GTPases and matrix fibers that controls fibroblast behavior during key phases of wound repair. We found that fiber-mediated spreading and migration required both Rac1 and ROCK activity, highlighting a role for these GTPases during the inflammatory phase of wound repair (Figs. 2, 3). During the proliferative phase of wound repair, Rac1 and ROCK were both critical for network formation and proliferation of fibroblasts (Fig. 4). Finally, despite ample literature highlighting RhoA/ROCK activity as the driver of MF differentiation in 2D, here we show that Rac1 and Cdc42 were additionally important for the 3D differentiation and contractile function of MFs at late timepoints (Figs. 5, 6).

Beyond characterizing various stages of the wound repair program in fibroblasts, these results add to our understanding of fibroblast-ECM interactions in 3D tissues which occurs throughout developmental processes, ECM homeostasis, and fibrotic disease.<sup>31</sup> First, we propose a developing mechanism for cell spreading in 3D fibrous environments whereby matrix fibers drive the initiation of thin nascent protrusions in a Rac1 dependent manner (Fig. 2), followed by RhoA/ROCK dependent expansion of these protrusions into thicker, spindle-like structures containing actin stress fibers (Fig. 3, Supplemental Fig. 1B, C). These results suggest that the previously associated morphologies established in 2D studies (whereby Rac1 drives lamellipodium creation, Cdc42 drives filopodia, and RhoA/ROCK drive stress fiber development) does not directly translate to more complex 3D and fibrous environments. More specifically, steric hindrance from surrounding matrix in 3D appears to prevent the formation of flat sheet-like actin structures comprising lamellipodia, instead favoring the formation of protrusions more reminiscent of large filopodia. Importantly, and quite distinct from 2D findings, these protrusions appear to require Rac1 activity and are not Cdc42 dependent. Fibers appear to provide contact guidance cues and direct localized Rac1 activity, perhaps in a similar fashion to our previous studies microcontact printing adhesive lines of fibronectin.<sup>73</sup>

Secondly, while prior work suggests that RhoA/ROCK and Rac1 signaling are in opposition in 2D,<sup>52,60</sup> these results suggest that they work in concert to support cell spreading and downstream actomyosin-dependent processes (eg. migration, proliferation, multicellular network formation, MF differentiation,

and contractile force generation). Indeed, the independence of ROCK and Rac1 in 2D is notable; in these contexts Rac1 inhibition prevents the formation of protrusions<sup>21</sup> but does not hinder the generation of F-actin rich stress fibers (Supplemental Fig. 1A). This is likely through elevated RhoA/ROCK activity in situations where Rac1 is absent,<sup>52</sup> in addition to the lack of steric hindrance from a surrounding 3D matrix. In contrast, protrusion formation appears to be a prerequisite for stress fiber generation in 3D (Figs. 2, 5, Supplemental Fig. 1B). However, as evidenced by the low spread area despite an increased number of nascent protrusions in Y-27632 treated conditions (Figs. 2, 3), protrusion formation appears to be necessary but not sufficient for stress fiber generation in 3D. Consequently, we hypothesize that insufficient coordination between Rac1 and ROCK is the primary reason for limited spreading in amorphous nonfibrous 3D hydrogels<sup>44</sup> (Figs. 1, 2, 3); a lack of ligand presenting guidance cues in 3D hinders Rac1 activation, preventing the formation of nascent protrusions which serve as scaffolds for downstream actin polymerization and ROCK-dependent stress fiber generation. Indeed, we did observe stress fibers in NSC-27632 treated cultures which were allowed to generate protrusions prior to dosing on day 5 (Fig. 5, Supplemental Fig. 1C), suggesting that Rac1 is needed before but not during stress fiber development in 3D.

Beyond contributing to a developing understanding of 3D mechanosensing, our work also has implications for the treatment of chronic wounds and fibrotic diseases. In the context of wound repair, material-based strategies have emerged as a promising tool to accelerate healing but have yet to be fully realized.<sup>23</sup> Our documentation of increased fibroblast migration, proliferation, and matrix remodeling in the presence of matrix fibers supports prior work showing the benefit of fibrous scaffolds in treating dermal, orthopedic, and cardiac wounds.<sup>9,25,56</sup> Importantly, emerging hydrogel technologies have numerous benefits (injectability, viscoelasticity, swelling capacity, non-fouling properties, etc.) but typically lack fibrous microstructure; our fiber-reinforcement technique is compatible across hydrogel platforms<sup>44</sup> and can be paired with developing technologies to enhance cell infiltration, spreading, and proliferation responses if desired. Furthermore, the complex dynamics of wound healing *in vivo* suggests differential adhesive and cytoskeletal states of fibroblasts depending on their required function—optimizing wound healing may require modulating Rho GTPases through cell engineering or dynamic material cues rather than a single material with a statically defined set of properties and resultant cell states.<sup>34</sup>

In contrast, it would be advantageous to prevent fibroblast migration, proliferation, and MF differentiation in the context of fibrotic diseases. Our results show that inhibiting any of the key cytoskeletal regulators was insufficient in preventing 3D MF differentiation in the presence of TGF- $\beta$ 1 and matrix fibers (Fig. 5), particularly after fibroblasts have proliferated and formed cell-cell junctions (Supplemental Fig. 1C), as occurs in clinically detectable fibrosis. Indeed, fibroblasts undergoing MF differentiation at late timepoints appeared to be resistant to pharmacologies when compared to immediate dosing of freshly encapsulated fibroblasts, where the effect of fibers on cell spreading (Fig. 2), proliferation (Fig. 4d), and network formation (Fig. 4b) was reversed under ROCK and Rac1 inhibition. Pharmacologic resistance may be one reason why drugs targeting mechanosensitive pathways have yet to be realized for the treatment of fibrotic disease, despite the well-established requirement of cell-matrix signaling for MF differentiation in 2D over short time scales.<sup>65</sup> It is also important to note that we used pharmacologic agents to disrupt ROCK, Rac1, and Cdc42 activity in this work; therefore it is possible that more elegant technologies which inhibit protein synthesis (siRNA, CRISPR knockouts) may have more pronounced effects and should be explored in future work.

Importantly, this work is not without limitations. We did not explore how matrix fibers influence 3D Rac1 activity at the subcellular level, or a detailed mechanism by which nascent protrusions develop into larger 3D cytoskeletal structures. Our observation that Cdc42 inhibition promoted 3D migration is discordant with findings from 2D models, perhaps arising from an interplay between Cdc42 and matrix metalloproteinase (MMP) activity,<sup>15</sup> which would be inconsequential in 2D given that matrix degradation is not required for migration in such contexts.<sup>78</sup> Further development of optogenetic tools, live activity reporters, and high-resolution timelapse imaging could enable future exploration and quantification of these complex and dynamic 3D cytoskeletal processes.<sup>43</sup> Furthermore, recent work from our lab and others has demonstrated that cell-derived ECM is rapidly deposited in 3D hydrogels<sup>41,42</sup>; we cannot exclude the potential for changes in adhesive ligand density across conditions over time, or for potential differences in integrin engagement to RGD-presenting fibers compared to cell-secreted fibronectin. Emerging technologies such as metabolic labeling<sup>41</sup> may allow for quantification and investigation of adhesive ligand-specific effects. Finally, RGD-presenting fibers and a polymeric gel were utilized to model the biphasic structure (adhesive fibrillar proteins and degradable gel-like proteoglycans) present *in vivo*; we present this material as a

reductionist approach to mimicking a complex physiologic stromal ECM. Future material development will be required to capture the heterogeneity of matrix proteins (e.g. collagen, elastin, fibronectin) and mechanical properties present in diverse tissue structures *in vivo*.

In summary, here we utilized a fibrous hydrogel model to explore the stimulatory effects of matrix fibers on fibroblast phenotype and documented the role of Rho GTPases during key cell processes during wound healing. These results emphasize the need to model complex biological processes, such as wound healing or fibrosis, in distinct cellular phases. Indeed, the timing of pharmacologic treatment is likely to have differing effects depending on the stage of the physiologic process being modeled. Further development of bioengineering tools which offer on-demand changes to the matrix- or cell-state will be a critical next step. Future work should also explore the role that other cell types (macrophages, endothelial cells, and mesenchymal stem cells) play during the wound healing process and whether they are influenced by fibers through similar mechanisms. Moreover, given the differences in mechanosensing between 2D, 3D, and 3D fibrous environments, this work motivates the development and implementation of biomimetic models which can elucidate physiologic understanding and support therapeutic translation.

## SUPPLEMENTARY INFORMATION

The online version contains supplementary material available at <https://doi.org/10.1007/s12195-021-00698-5>.

## ACKNOWLEDGMENTS

We thank Dr. Eric S. White (University of Michigan) for providing the human fibroblasts employed in these studies.

## AUTHOR CONTRIBUTIONS

D.L.M and B.M.B conceived the experiments, supervised the project, and wrote the manuscript. D.L.M. designed and performed the experiments. A.L. conducted data analysis for Figs. 2, 3 and 4. H.L.H created and aided in the use of a custom Matlab script for cell migration analysis. All authors edited and approved the manuscript.

## FUNDING

This work was supported in part by the National Institutes of Health (HL124322, EB030474). DLM acknowledges financial support from the National Science Foundation Graduate Research Fellowship Program (DGE1256260).

## CONFLICT OF INTEREST

D.L.M, A.T.L, H.L.H, and B.M.B declare that they have no conflicts of interest.

## DATA AVAILABILITY

Datasets are available on request: the raw data supporting the conclusions of this article will be made available by the authors, without undue reservation, by request.

## ETHICAL STANDARDS

No human or animal studies were carried out by the authors for this article.

## REFERENCES

- <sup>1</sup>Baker, B. M., et al. The potential to improve cell infiltration in composite fiber-aligned electrospun scaffolds by the selective removal of sacrificial fibers. *Biomaterials*. 29:2348–2358, 2008.
- <sup>2</sup>Balestrini, J. L., S. Chaudhry, V. Sarrazy, A. Koehler, and B. Hinz. The mechanical memory of lung myofibroblasts. *Integr. Biol.* 4:410–421, 2012.
- <sup>3</sup>Barker, T. H., and A. J. Engler. The provisional matrix: setting the stage for tissue repair outcomes. *Matrix Biol.* 60–61:1–4, 2017. <https://doi.org/10.1016/j.matbio.2017.04.003>.
- <sup>4</sup>Bellis, S. L. Advantages of RGD peptides for directing cell association with biomaterials. *Biomaterials*. 32:4205–4210, 2011. <https://doi.org/10.1016/j.biomaterials.2011.02.029>.
- <sup>5</sup>Bochaton Piallat, M.-L., G. Gabbiani, and B. Hinz. The myofibroblast in wound healing and fibrosis: answered and unanswered questions. *F1000 Res.* 2016. <https://doi.org/10.12688/f1000research.8190.1>.
- <sup>6</sup>Califano, J. P., and C. A. Reinhart-King. A balance of substrate mechanics and matrix chemistry regulates endothelial cell network assembly. *Cell. Mol. Bioeng.* 1:122–132, 2008.
- <sup>7</sup>Castella, L. F., L. Buscemi, C. Godbout, J. J. Meister, and B. Hinz. A new lock-step mechanism of matrix remodelling based on subcellular contractile events. *J. Cell Sci.* 123:1751–1760, 2010.
- <sup>8</sup>Choi, S. S., et al. Activation of Rac1 promotes hedgehog-mediated acquisition of the myofibroblastic phenotype in rat and human hepatic stellate cells. *Hepatology*. 52:278–290, 2010.
- <sup>9</sup>Coburn, J., et al. Biomimetics of the extracellular matrix: an integrated three-dimensional fiber-hydrogel composite for cartilage tissue engineering. *Smart Struct. Syst.* 7:213–222, 2011.
- <sup>10</sup>Cox, T. R., and J. T. Erler. Remodeling and homeostasis of the extracellular matrix: implications for fibrotic diseases and cancer. *Dis. Model. Mech.* 4:165–178, 2011.
- <sup>11</sup>Darby, I., O. Skalli, and G. Gabbiani. Alpha-smooth muscle actin is transiently expressed by myofibroblasts during experimental wound healing. *Lab. Investig.* 63:21–29, 1990.
- <sup>12</sup>Darby, I. A., and T. D. Hewitson. Fibroblast differentiation in wound healing and fibrosis. *Int. Rev. Cytol.* 257:143–179, 2007.
- <sup>13</sup>Davidson, C. D., et al. Myofibroblast activation in synthetic fibrous matrices composed of dextran vinyl sulfone. *Acta Biomater.* 105:78–86, 2020.
- <sup>14</sup>Davidson, C. D., W. Y. Wang, I. Zaimi, D. K. P. Jayco, and B. M. Baker. Cell force-mediated matrix reorganization underlies multicellular network assembly. *Sci. Rep.* 2019. <https://doi.org/10.1038/s41598-018-37044-1>.
- <sup>15</sup>Deroanne, C. F., et al. Cdc42 downregulates MMP-1 expression by inhibiting the ERK1/2 pathway. *J. Cell Sci.* 118:1173–1183, 2005.
- <sup>16</sup>Edlund, S., M. Landström, C. H. Heldin, and P. Aspenström. Transforming growth factor- $\beta$ -induced mobilization of actin cytoskeleton requires signaling by small GTPases Cdc42 and RhoA. *Mol. Biol. Cell.* 13:902–914, 2002.
- <sup>17</sup>Fiore, V. F., et al. Integrin  $\alpha$  v  $\beta$  3 drives fibroblast contraction and strain stiffening of soft provisional extracellular matrix during progressive fibrosis. *JCI Insight.* 3:1–35, 2018.
- <sup>18</sup>Follonier, L., S. Schaub, J.-J. Meister, and B. Hinz. Myofibroblast communication is controlled by intercellular mechanical coupling. *J. Cell Sci.* 121:3305–3316, 2008.
- <sup>19</sup>Frantz, C., K. M. Stewart, and V. M. Weaver. The extracellular matrix at a glance. *J. Cell Sci.* 123:4195–4200, 2010. <https://doi.org/10.1242/jcs.023820>.
- <sup>20</sup>Gabbiani, G., C. Chaponnier, and I. Huttner. Cytoplasmic filaments and gap junctions in epithelial cells and myofibroblasts during wound healing. *J. Cell Biol.* 76:561–568, 1978.
- <sup>21</sup>Ge, J., et al. RhoA, Rac1 and Cdc42 differentially regulate  $\alpha$ SMA and collagen I expression in mesenchymal stem cells. *J. Biol. Chem.* 293(24):9358–9369, 2018.
- <sup>22</sup>Ghajar, C. M., et al. The effect of matrix density on the regulation of 3-D capillary morphogenesis. *Biophys. J.* 94:1930–1941, 2008.
- <sup>23</sup>Griffin, D. R., W. M. Weaver, P. O. Scumpia, D. Di Carlo, and T. Segura. Accelerated wound healing by injectable microporous gel scaffolds assembled from annealed building blocks. *Nat. Mater.* 14:737–744, 2015.
- <sup>24</sup>Gunatillake, P. A., R. Adhikari, and N. Gadegaard. Biodegradable synthetic polymers for tissue engineering. *Eur. Cells Mater.* 5:1–16, 2003.
- <sup>25</sup>Hassiba, A. J., et al. Review of recent research on biomedical applications of electrospun polymer nanofibers for improved wound healing. *Nanomedicine.* 11:715–737, 2016.
- <sup>26</sup>Hinz, B. The role of myofibroblasts in wound healing. *Curr. Res. Transl. Med.* 64:171–177, 2016. <https://doi.org/10.1016/j.retram.2016.09.003>.
- <sup>27</sup>Hinz, B. Formation and function of the myofibroblast during tissue repair. *J. Investig. Dermatol.* 127:526–537, 2007. <https://doi.org/10.1038/sj.jid.5700613>.

- <sup>28</sup>Hinz, B., and G. Gabbiani. Cell-matrix and cell-cell contacts of myofibroblasts: role in connective tissue remodeling. *Thromb. Haemost.* 90:993–1002, 2003.
- <sup>29</sup>Hinz, B., C. A. Mcculloch, and N. M. Coelho. Mechanical regulation of myofibroblast phenocconversion and collagen contraction. *Exp. Cell Res.* 379:119–128, 2019. <https://doi.org/10.1016/j.yexcr.2019.03.027>.
- <sup>30</sup>Huang, X., et al. Matrix stiffness-induced myofibroblast differentiation is mediated by intrinsic mechanotransduction. *Am. J. Respir. Cell Mol. Biol.* 47:340–348, 2012.
- <sup>31</sup>Humphrey, J. D., E. R. Dufresne, and M. A. Schwartz. Mechanotransduction and extracellular matrix homeostasis. *Nat. Rev. Mol. Cell Biol.* 15:802–812, 2014. <https://doi.org/10.1038/nrm3896>.
- <sup>32</sup>Igata, T., et al. Up-regulated type I collagen expression by the inhibition of Rac1 signaling pathway in human dermal fibroblasts. *Biochem. Biophys. Res. Commun.* 393:101–105, 2010. <https://doi.org/10.1016/j.bbrc.2010.01.090>.
- <sup>33</sup>Kendall, R. T., and C. A. Feghali-Bostwick. Fibroblasts in fibrosis: novel roles and mediators. *Front. Pharmacol.* 5:123, 2014.
- <sup>34</sup>Kim, S., M. Uroz, J. L. Bays, and C. S. Chen. Harnessing mechanobiology for tissue engineering. *Dev. Cell.* 56:180–191, 2021. <https://doi.org/10.1016/j.devcel.2020.12.017>.
- <sup>35</sup>Klingberg, F., B. Hinz, and E. S. White. The myofibroblast matrix: implications for tissue repair and fibrosis. *J. Pathol.* 229:298–309, 2013.
- <sup>36</sup>Leong, W. S., S. C. Wu, K. Ng, and L. P. Tan. Electrospun 3D multi-scale fibrous scaffold for enhanced human dermal fibroblast infiltration. *Int. J. Bioprint.* 2:81–92, 2016.
- <sup>37</sup>Li, L., J. Eyckmans, and C. S. Chen. Designer biomaterials for mechanobiology. *Nat. Mater.* 16:1164–1168, 2017.
- <sup>38</sup>Liang, C. C., A. Y. Park, and J. L. Guan. In vitro scratch assay: a convenient and inexpensive method for analysis of cell migration in vitro. *Nat. Protoc.* 2:329–333, 2007.
- <sup>39</sup>Liu, S., et al. Role of Rac1 in a bleomycin-induced scleroderma model using fibroblast-specific Rac1-knockout mice. *Arthritis Rheum.* 58:2189–2195, 2008.
- <sup>40</sup>Liu, S., M. Kapoor, and A. Leask. Rac1 expression by fibroblasts is required for tissue repair in vivo. *Am. J. Pathol.* 174:1847–1856, 2009. <https://doi.org/10.2353/ajpath.2009.080779>.
- <sup>41</sup>Loebel, C., M. Y. Kwon, C. Wang, L. Han, R. L. Mauck, and J. A. Burdick. Metabolic labeling to probe the spatiotemporal accumulation of matrix at the chondrocyte-hydrogel interface. *Adv. Funct. Mater.* 1909802:1–10, 2020.
- <sup>42</sup>Matera, D. L., et al. Microengineered 3D pulmonary interstitial mimetics highlight a critical role for matrix degradation in myofibroblast differentiation. *Sci. Adv.* 6:1–15, 2020.
- <sup>43</sup>Matera, D. L., W. Y. Wang, and B. M. Baker. New directions and dimensions for bioengineered models of fibrosis. *Nat. Rev. Mater.* 2021. <https://doi.org/10.1038/s41578-021-00288-x>.
- <sup>44</sup>Matera, D. L., W. Y. Wang, M. R. Smith, A. Shikanov, and B. M. Baker. Fiber density modulates cell spreading in 3D interstitial matrix mimetics. *ACS Biomater. Sci. Eng.* 5:2965–2975, 2019.
- <sup>45</sup>Nakagawa, S., P. Pawelek, and F. Grinnell. Long-term culture of fibroblasts in contracted collagen gels: effects on cell growth and biosynthetic activity. *J. Investig. Dermatol.* 93:792–798, 1989. <https://doi.org/10.1111/1523-1747.ep12284425>.
- <sup>46</sup>Nobes, C. D. Rho GTPases and cell migration-fibroblast wound. *Cell.* 325:441–449, 2000.
- <sup>47</sup>O'Connor, J. W., and E. W. Gomez. Cell adhesion and shape regulate TGF-beta1-induced epithelial-myofibroblast transition via MRTF-A signaling. *PLoS ONE.* 8:1–11, 2013.
- <sup>48</sup>Oh, R. S., A. J. Haak, K. M. J. Smith, and G. Ligresti. RNAi screening identifies a mechanosensitive ROCK-JAK2-STAT3 network central to myofibroblast activation. *J. Cell Sci.* 131:jcs209932, 2018.
- <sup>49</sup>Olczyk, P., L. Mencner, and K. Komosinska-Vashev. Diverse roles of Heparan Sulfate and Heparin in wound repair. *Bio. Med. Res. Int.* 1–7, 2015. <https://doi.org/10.1155/2015/549417>.
- <sup>50</sup>Ortega, S., M. Ittmann, S. H. Tsang, M. Ehrlich, and C. Basilico. Neuronal defects and delayed wound healing in mice lacking fibroblast growth factor 2. *Proc. Natl. Acad. Sci. USA.* 95:5672–5677, 1998.
- <sup>51</sup>Pathak, A., and S. Kumar. Biophysical regulation of tumor cell invasion: moving beyond matrix stiffness. *Integr. Biol.* 3:267–278, 2011.
- <sup>52</sup>Pertz, O., L. Hodgson, R. L. Klemke, and K. M. Hahn. Spatiotemporal dynamics of RhoA activity in migrating cells. *Nature.* 440:1069–1072, 2006.
- <sup>53</sup>Pittet, P., K. Lee, A. J. Kulik, J.-J. Meister, and B. Hinz. Fibrogenic fibroblasts increase intercellular adhesion strength by reinforcing individual OB-cadherin bonds. *J. Cell Sci.* 121:877–886, 2008. <https://doi.org/10.1242/jcs.024877>.
- <sup>54</sup>Pothula, S., H. E. P. Bazan, and G. Chandrasekher. Regulation of cdc42 expression and signaling is critical for promoting corneal epithelial wound healing. *Investig. Ophthalmol. Vis. Sci.* 54:5343–5352, 2013.
- <sup>55</sup>Provenzano, P. P., K. W. Eliceiri, D. R. Inman, and P. J. Keely. Engineering three-dimensional collagen matrices to provide contact guidance during 3D cell migration. *Curr. Protoc. Cell Biol.* 1–11, 2010.
- <sup>56</sup>Ravichandran, R., J. R. Venugopal, S. Sundarajan, S. Mukherjee, R. Sridhar, and S. Ramakrishna. Minimally invasive injectable short nanofibers of poly(glycerol sebacate) for cardiac tissue engineering. *Nanotechnology.* 23:385102, 2012.
- <sup>57</sup>Riching, K. M., et al. 3D collagen alignment limits protrusions to enhance breast cancer cell persistence. *Biophys. J.* 107:2546–2558, 2015. <https://doi.org/10.1016/j.bpj.2014.10.035>.
- <sup>58</sup>Ridley, A. J. Rho GTPases and cell migration. *J. Cell Sci.* 114:2713–2722, 2001.
- <sup>59</sup>Russell, S. M., and G. Carta. Mesh size of charged polyacrylamide hydrogels from partitioning measurements. *Ind. Eng. Chem. Res.* 44:8213–8217, 2005.
- <sup>60</sup>Sander, E. E., J. P. Ten Klooster, S. Van Delft, R. A. Van Der Kammen, and J. G. Collard. Rac downregulates Rho activity: reciprocal balance between both GTPases determines cellular morphology and migratory behavior. *J. Cell Biol.* 147:1009–1021, 1999.
- <sup>61</sup>Scharenberg, M. A., et al. TGF- $\beta$ -induced differentiation into myofibroblasts involves specific regulation of two MKL1 isoforms. *J. Cell Sci.* 127:1079–1091, 2014.
- <sup>62</sup>Shi-wen, X., et al. Rac inhibition reverses the phenotype of fibrotic fibroblasts. *PLoS ONE.* 4:1–9, 2009.
- <sup>63</sup>Shimizu, Y., et al. Contribution of small GTPase Rho and its target protein ROCK in a murine model of lung fibrosis. *Am. J. Respir. Crit. Care Med.* 163:210–217, 2001.
- <sup>64</sup>Singer, A. J., and R. A. F. Clark. Cutaneous wound healing. *N. Engl. J. Med.* 341:738–746, 1999. <https://doi.org/10.1056/NEJM199909023411006>.

- <sup>65</sup>Smithmyer, M. E., L. A. Sawicki, and A. M. Kloxin. Hydrogel scaffolds as in vitro models to study fibroblast activation in wound healing and disease. *Biomater. Sci.* 2:634–650, 2014.
- <sup>66</sup>Sukmana, I., and P. Vermette. Polymer fibers as contact guidance to orient microvascularization in a 3D environment. *J. Biomed. Mater. Res. Part A.* 92:1587–1597, 2010.
- <sup>67</sup>Tapon, N., and A. Hall. Rho, Rac and Cdc42 GTPases regulate the organization of the actin cytoskeleton. *Curr. Opin. Cell Biol.* 9:86–92, 1997.
- <sup>68</sup>Tomasek, J. J., G. Gabbiani, B. Hinz, C. Chaponnier, and R. A. Brown. Myofibroblasts and mechano: regulation of connective tissue remodelling. *Nat. Rev. Mol. Cell Biol.* 3:349–363, 2002.
- <sup>69</sup>Tschumperlin, D. J. Fibroblasts and the ground they walk on. *Physiology.* 28:380–390, 2013.
- <sup>70</sup>Vogel, V. Unraveling the mechanobiology of extracellular matrix. *Annu. Rev. Physiol.* 80:353–387, 2018.
- <sup>71</sup>Vyalov, S. L., G. Gabbiani, and Y. Kapanci. Rat alveolar myofibroblasts acquire smooth muscle actin expression during bleomycin-induced pulmonary fibrosis. *Am. J. Pathol.* 143:1754–1765, 1993.
- <sup>72</sup>Walraven, M., and B. Hinz. Therapeutic approaches to control tissue repair and fibrosis: Extracellular matrix as a game changer. *Matrix Biol.* 71–72:205–224, 2018. <https://doi.org/10.1016/j.matbio.2018.02.020>.
- <sup>73</sup>Wang, W. Y., et al. Extracellular matrix alignment dictates the organization of focal adhesions and directs uniaxial cell migration. *APL Bioeng.* 2018. <https://doi.org/10.1063/1.5052239>.
- <sup>74</sup>Wang, X., B. Ding, and B. Li. Biomimetic electrospun nanofibrous structures for tissue engineering. *Mater. Today.* 16:229–241, 2013. <https://doi.org/10.1016/j.mattod.2013.06.005>.
- <sup>75</sup>Wells, A. U., and T. M. Maher. Update in interstitial lung disease 2016. *Am. J. Respir. Crit. Care Med.* 196:132–138, 2017.
- <sup>76</sup>Wirtz, D. Intracellular mechanics of migrating fibroblasts. *Mol. Biol. Cell.* 15:5318–5328, 2004.
- <sup>77</sup>Wynn, T. A. Cellular and molecular mechanisms of fibrosis. *J. Pathol.* 214:199–210, 2008.
- <sup>78</sup>Yamada, K. M., and M. Sixt. Mechanisms of 3D cell migration. *Nat. Rev. Mol. Cell Biol.* 2019. <https://doi.org/10.1038/s41580-019-0172-9>.
- <sup>79</sup>Yasui, T., R. Tanaka, E. Hase, S. Fukushima, and T. Araki. In vivo time-lapse imaging of skin burn wound healing using second-harmonic generation microscopy. *Multiphot. Microsc. Biomed. Sci. XIV.* 8948:89480B, 2014.
- <sup>80</sup>Yee, H. F., A. C. Melton, and B. N. Tran. RhoA/Rho-associated kinase mediates fibroblast contractile force generation. *Biochem. Biophys. Res. Commun.* 280:1340–1345, 2001.

**Publisher's Note** Springer Nature remains neutral with regard to jurisdictional claims in published maps and institutional affiliations.